Molecular Physics, 2013
Vol. 111, Nos. 9–11, 1497–1510, http://dx.doi.org/10.1080/00268976.2013.796070

INVITED ARTICLE

Local vibrational modes of the formic acid dimer – the strength of the double hydrogen bond

R. Kalescky, E. Kraka and D. Cremer*

Department of Chemistry, Southern Methodist University, 3215 Daniel Avenue, Dallas, Texas 75275, USA

(*Received 13 February 2013; final version received 8 April 2013*)

The 24 normal and 24 local vibrational modes of the formic acid dimer formed by two trans formic acid monomers to a ring (**TT1**) are analysed utilising preferentially experimental frequencies, but also CCSD(T)/CBS and ωB97X-D harmonic vibrational frequencies. The local hydrogen bond (HB) stretching frequencies are at 676 cm^{-1} and by this 482 and 412 cm^{-1} higher compared to the measured symmetric and asymmetric HB stretching frequencies at 264 and 194 cm^{-1}. The adiabatic connection scheme between local and normal vibrational modes reveals that the lowering is due to the topology of dimer **TT1**, mass coupling, and avoided crossings involving the $H\cdots OC$ bending modes. The HB local mode stretching force constant is related to the strength of the HB whereas the normal mode stretching force constant and frequency lead to an erroneous underestimation of the HB strength. The HB in **TT1** is stabilised by electron delocalisation in the O=C–O units fostered by forming a ring via double HBs. This implies that the CO apart from the OH local stretching frequencies reflect the strength of the HB via their red or blue shifts relative to their corresponding values in trans formic acid.

Keywords: formic acid dimer; vibrational spectra; local vibrational modes; hydrogen bond stretching frequencies; hydrogen bond strength; red and blue shifts of stretching modes

1. Introduction

Formic acid (FA), as the smallest organic acid, is a suitable model to study dimer formation via hydrogen bonding (HB) [1,2] where the conformation of the monomer plays an important role. In trans formic acid, the two H atoms are in E position and in the corresponding cis form in Z position of the C–O bond. According to experiment, the energy of the cis form is 3.9 kcal/mol higher in energy [3,4] and converts back to the trans form via tunnelling through a torsional barrier of 13.8 kcal/mol [5–8]. The most stable formic acid dimer (FAD) is formed from two trans forms (henceforth called **TT1**., see Figure 1(a) and 1(b)), which are held together by two HBs (double HB), thus forming a planar 8-membered ring. Other trans–trans forms can also form HBs of the type $C = O\cdots H - C$ to form 8-, 7-, or 6-membered rings closed by double HB. Trans–cis and cis–cis dimers involve the cis form of FA and, therefore, they can only form 7-, 6-, or 5-membered rings. FADs with one HB are significantly less stable and there are up to 18 cyclic and acyclic FAD forms with double HB or single HB that have been discussed in the literature [9–35].

H-bonding between two or more FA (or other carboxylic acid) molecules has been found to produce nucleating agents for atmospheric aerosols where the thermodynamic stability of these complexes is determined by the strength of double HBs [36,37]. A key step toward understanding this process is understanding the nature of the H-bonding of these molecules, which is important as the distinction between molecule, macromolecule, and particle becomes less defined. Additionally, FA is a relatively weak acid ($pK_a = 3.77$) due to the stability imparted by double H-bonding and is known to affect reactions in clouds that are pH-dependent [38,39].

In view of the important role of FAD for the understanding of the HB, it is not surprising that the number of quantum chemical investigations [9–22] outnumbers the experimental ones [23–35]. However in recent years, improved experimental techniques, as for example advanced versions of matrix isolation spectroscopy and supersonic jet expansions, have played an important role to experimentally determine the properties of the FAD, where specifically the work of Khriachtchev and co-workers [29–32] and Suhm and co-workers [33–35] has to be mentioned. These investigations are driven by a general interest into revealing the nature of the HB as it is documented in several monographs [1,2,40–43] and numerous review articles only some of which can be mentioned here [44–50].

In this work, we will investigate the strength of the double HB in FAD **TT1** using experimental normal mode frequencies [35], converting these into local mode frequencies [51–54], and then, with the help of the local OH stretching force constants, determine the relative strength of the OH donor and OH acceptor bonds in FAD structure **TT1** [53,55]. This line of investigation, we have recently applied

*Corresponding author. Email: dieter.cremer@gmail.com

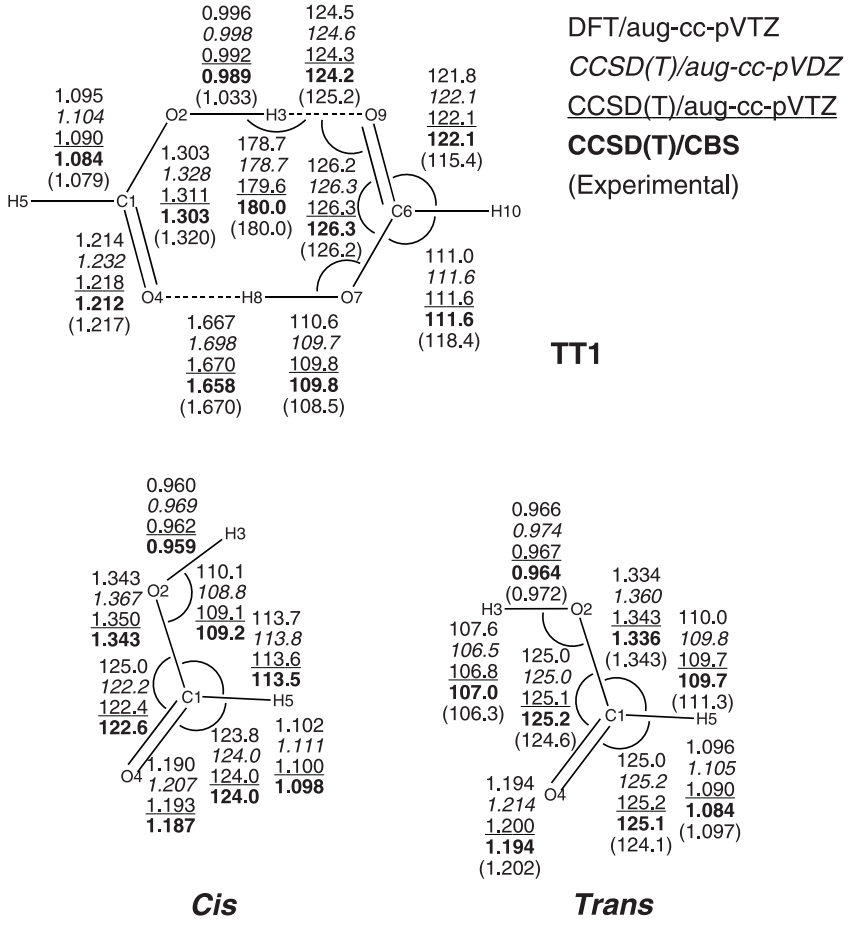

(a)

Figure 1. Geometries of (a) cis formic acid, trans formic acid, and the FAD **TT1**.; (b) reference molecules **TT2**, **TC1**, **TC2**, and **CC1**. Bond lengths in Å and angles in degrees. The numbering of atoms is used throughout this work.

for the first time for the investigation of the water dimer [56] where we could demonstrate that the HB stretching frequency measured by experimentalists at 143 cm^{-1} corresponds to a local mode stretching frequency of 390 cm^{-1}, which is better in line with a binding energy of ΔE of 5.0 kcal/mol in this case and can be directly compared with local mode stretching frequencies of HBs in other complexes [56]. We will use local mode stretching force constants to determine OH and CO bond orders [55], and to investigate structural changes, red (blue) shifts in the vibrational frequencies caused by double HBs or normal HBs, and the actual properties of double HBs as they are reflected by the corresponding local mode properties. For this purpose, we will relate normal and local modes by an adiabatic connection scheme (ACS), which we recently introduced to understand mass coupling, avoided crossings, and anharmonicity effects influencing the conversion of local modes into normal modes [53,56].

2. Computational methods

Local vibrational frequencies ω_a (a for adiabatic) and local force constants k_a were calculated from normal vibrational frequencies using the procedure described by Konkoli and Cremer [51]. These authors have shown that, by solving mass-decoupled Euler-Lagrange equations, local modes $\mathbf{a_n}$ associated with internal coordinate displacements q_n are obtained. For the practical determination of vectors $\mathbf{a_n}$, the normal modes $\mathbf{d_n}$ (expressed in terms of internal coordinates) have to be determined by solving the Wilson equation:

$$\mathbf{F^q D} = \mathbf{G}^{-1}\mathbf{D\Lambda}, \tag{1}$$

where $\mathbf{F}^q$ is the force constant matrix, $\mathbf{G}$ the Wilson matrix ($\mathbf{G}^{-1}$ gives the kinetic energy in terms of q-coordinates), $\mathbf{\Lambda}$ is the diagonal matrix of eigenvalues $\lambda_\mu = 4\pi^2 c^2 \omega_\mu^2$ (ω_μ:

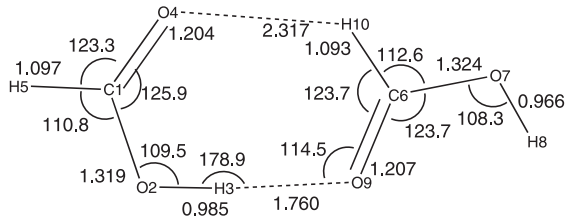

TT2

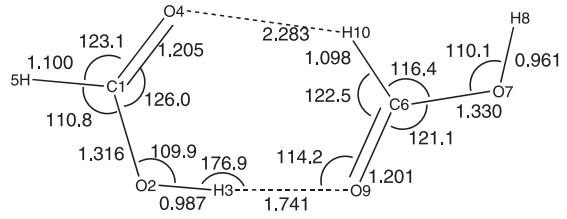

TC1

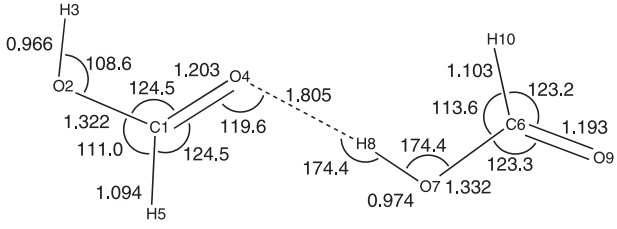

TC2

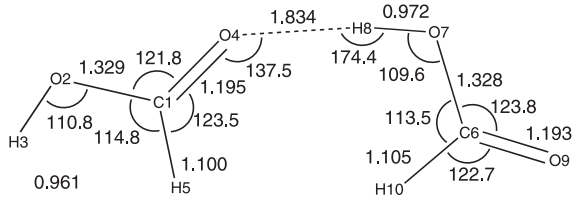

CC1

(b)

Figure 1. (Continued)

normal mode frequencies), and matrix **D** collects the normal mode vectors $\mathbf{d}_\mu$ as column vectors. If $\mathbf{K} = \mathbf{D}^\dagger \mathbf{F^q D}$ gives the diagonalised force constant matrix, then the local mode vectors are defined by

$$\mathbf{a}_n = \frac{\mathbf{K}^{-1}\mathbf{d}_n^\dagger}{\mathbf{d}_n\mathbf{K}^{-1}\mathbf{d}_n^\dagger} \tag{2}$$

and the local mode force constants for a given mode n by

$$k_{a,n} = \mathbf{a}_n^\dagger \mathbf{K} \mathbf{a}_n = (\mathbf{d}_n\mathbf{K}^{-1}\mathbf{d}_n^\dagger)^{-1} \tag{3}$$

with $\mathbf{d}_n$ now being row vectors of **D**. The local mode frequencies ω_a associated with k_a are related to the normal mode frequencies via the coupling frequencies ω_{coup}, i.e. $\omega_\mu = \omega_a + \omega_{coup}$.

In recent work, we have shown that (i) these local modes are the only local modes directly related to the normal modes [53,54]; (ii) the reciprocal force constants k_a are equal to the compliance constants first mentioned by Decius [57] to be used as possible parameters to describe local mode properties. Although a mathematical reasoning for the compliance constants was given by Decius and others [57–59], the physical relevance of them becomes only clear with the help of the properties of the local modes [53,54]; (iii) one can relate the local mode frequencies to the normal mode frequencies by using an ACS. Such a scheme reveals how the normal modes are generated via coupling between the local modes and the influence of mass couplings, symmetry, and avoided crossings [53,54,56].

Using the experimental frequencies ω_μ of **TT1** given in the literature [35], local mode frequencies ω_a were derived according to the procedure given by Cremer and coworkers [60]. Once the local modes were determined, the normal vibrational modes were characterised in terms of local vibrational modes using the CNM (characterisation of normal modes) approach of Konkoli and Cremer [52]. The ACS method of [53] was used to relate frequencies ω_a to ω_μ and to determine the coupling frequencies $\omega_{coup} = \omega_\mu - \omega_a$, which provide a cumulative measure for the strength of coupling between local modes. For the generation of the ACS, a perturbation formula is used, in which a scaling parameter λ switches on mass coupling between the local modes to convert ω_a into ω_μ [53]. The frequencies are then presented as a function of λ where the ordering of frequencies is performed with the diabatic mode ordering method [61].

Equilibrium geometry, harmonic vibrational frequencies, and harmonic infrared intensities of FAD form **TT1**, and some other dimer forms used as references and shown in Figure 1(a) and 1(b) were calculated using the long-range corrected hybrid density functional ωB97X-D, which includes empirical dispersion corrections [62,63], in connection with the aug-cc-pVTZ basis set of Dunning [64,65]. For the investigation of the FAD complexes, the counterpoise correction was used to account for basis set superposition errors (BSSE) [66,67]. Sherrill and co-workers showed that for counterpoise-corrected ωB97X-D calculations, HB binding energies ΔE close to reliable CCSD(T) results are obtained [68].

For the purpose of getting accurate descriptions for the target system **TT1**, we employed CCSD(T) theory [69] in connection with Dunning's aug-cc-pVXZ (X = D, T) basis sets [64,65]. These calculations were the basis for extrapolating results to the CCSD(T) complete basis set (CCSD(T)/CBS) limit utilising a 2-point extrapolation formula [70]. BSSE corrections were also calculated at the

Table 1. The bond dissociation energy, enthalpy, and free energy and the entropy are given for the FADs. The entropies of the trans formic acid are 59.45, 59.33, 59.27, 59.28 cal/mol-K; those of cis formic acid 59.65, 59.51, 59.45, and 59.42 cal/mol K at the CCSD(T)/aug-cc-pVDZ, CCSD(T)/aug-cc-pVTZ, CCSD(T)/CBS, and ωB97XD/aug-cc-pVTZ levels of theory, respectively. BSSE corrections for **TT1, TT2, TC1, TC2,** and **CC1** at ωB97XD/aug-cc-pVTZ are 0.35, 0.22, 0.23, 0.20, and 0.20 kcal/mol, respectively. For **TT1**, the CCSD(T) BSSE corrections are 1.43 and 1.45 kcal/mol.

System FAD, FA	Method	ΔE [kcal/mol]	$\Delta H(298)$ [kcal/mol]	S, ΔS [cal/mol K]	$\Delta G(298)$ [kcal/mol]
TT1	CCSD(T)/aug-cc-pVDZ	−16.71	−14.95	80.76	−3.58
	CCSD(T)/aug-cc-pVTZ	−18.12	−16.38	80.15	−4.90
	CCSD(T)/CBS	−18.72	−16.98	79.90	−5.46
	ωB97XD/aug-cc-pVTZ	−17.11	−15.60	79.89	−4.08
TT2	ωB97XD/aug-cc-pVTZ	−10.09	−8.55	85.83	1.21
TC1	ωB97XD/aug-cc-pVTZ	−11.07	−9.44	85.41	0.48
TC2	ωB97XD/aug-cc-pVTZ	−8.09	−7.13	87.21	2.26
CC1	ωB97XD/aug-cc-pVTZ	−7.53	−6.59	88.42	2.49
T-C	CCSD(T)/aug-cc-pVDZ	−4.22	−4.03	−0.20	−3.97
	CCSD(T)/aug-cc-pVTZ	−4.27	−4.08	−0.18	−4.03
	CCSD(T)/CBS	−4.29	−4.10	−0.18	−4.05
	ωB97XD/aug-cc-pVTZ	−4.13	−3.97	−0.14	−3.93

CCSDT) level, however, not used to improve complex binding energies because they are unusually large (see Table 1). This is in line with the observations of other authors [71–73] and results from the fact that for highly correlated wavefunction methods calculated with incomplete basis sets, the intramolecular BSSE, which leads to artificial electron correlation effects, increases significantly the intermolecular BSSE thus significantly changing the convergence behaviour of the wavefunction method in dependence of the basis set. Therefore, we followed recommendations given in the literature and excluded BSSE corrections for the CCSD(T) results [73].

For the purpose of determining red and blue shifts in the vibrational frequencies of **TT1** upon complex formation, trans formic acid and cis formic acid were also investigated where the experimental frequencies $\omega_\mu(Exp)$ were taken from Marcoas and co-workers [74] and all other calculations were carried out in a similar way as for FAD. The differences $\Delta\omega = \omega(Exp) - \omega(CBS)$ obtained for FA and the FAD form **TT1** are dominated, but not equal to the anharmonicity effects of the frequencies. This is due to three other contributions to $\Delta\omega$. (i) The CBS frequencies obtained in this work will slightly differ from their true full CI/CBS values as a result of the extrapolation procedure used and some limitations of the CCSD(T) method. (ii) The CBS frequencies are obtained at the CBS equilibrium geometry r_e whereas the measured frequencies refer to the corresponding r_o and r_a geometries of the target molecules [75,76], Hence, $\Delta\omega$ depends also on this geometry effect. (iii) Only in a few cases, the experimental frequencies have been determined for the zero vibrational level ($v = 0$) whereas the values used in this work are red shifted due to the presence of *hot bands* [35]. All three effects make small, but significant contributions to $\Delta\omega$ thus excluding a precise determination of the anharmonicity effects, which are discussed here only in a qualitative manner.

The determination of the local modes and their properties is independent of the choice of the other coordinates [51]. This is no longer true when setting up the $3N - 6$ (N: number of atoms) local modes for the ACS. In the cases of FA and FAD, there are more than $3N - 6$ internal coordinates, which can be used to describe the molecular geometry. For example, in the case of FA $3N - 6 = 9$ whereas there are 10 internal coordinates if just bond lengths, bond angles, and bond dihedral angles are used (4 bond lengths, 4 bond angles, and 2 out-of-plane angles for the 2 H atoms). We solved this problem by eliminating one of the bond angles at C on the basis that the sum of bond angles at the C atom must be 360°, which makes the third XCY bond angle redundant. In a similar way, we approached the problem of defining 24 local modes and their associated internal coordinates in the case of **TT1** and other FADs. We included all bond lengths (plus any HB distance), the non-redundant bond angles, and a limited number of bond dihedral angles. The choice of the number of bond dihedral angles was facilitated by the fact that all FADs investigated form a ring. For any ring structure, the number of out-of-plane vibrational modes is given by the number of puckering coordinates [77–79]. Rather than using puckering coordinates, we defined the appropriate number of dihedral angles.

Local mode force constants k_a were used to determine OH, CH, and CO bond orders n. There is a continuous transition from electrostatic to covalent HBs. Parallel to this change, there is a reverse change in the nature of the $D - H$ single bond (D: donor), which is increasingly weakened with increasing interactions between H and acceptor (A), i.e. with increasing HB strength. The local stretching force constants k_a(DH) and k_a(HA) = k_a(HB) are sensitive to

the total density distribution enveloping the three atoms involved in HB and thereby they reflect all electrostatic and covalent contributions to HB, i.e. they present a measure of the intrinsic bond strength of both DH and HA interactions.

For any X–H bond (here X = O, C), we used a similar approach as described by Freindorf and co-workers [55], i.e. we used either ωB97X-D, CCSD(T), or experimental frequencies of FH ($n = 1$) and F-H-F$^-$ ($n = 0.5$) as references to set up a power relationship between bond order n and local mode stretching force constant k_a where for $k_a = 0$ the bond order $n = 0$ is required. The resulting bond orders were rescaled to obtain for the OH bond in the water molecule or the CH bond in the methane molecule the value $n = 1$. For the CO bonds, references are methanol ($n = 1$) and formaldehyde ($n = 2$). The experimental frequencies for all references have been taken from the literature (FH [80], F-H-F$^-$ [81], methanol [82], formaldehyde [82]).

3. Results and discussion

Results of this investigation are summarised in Tables 1 (energies), 2 (harmonic CCSD(T) frequencies, 3 (decomposition of the normal modes of **TT1** into local modes), 4 (experimental local mode frequencies), 5 (X–H, C–O, C=O bond orders) and Figures 1(a), 1(b) (geometries), 2 (6 intermonomer modes of **TT1**), 3 (mode decomposition diagram for **TT1**), 4(a), 4(b), 4(c) (ACS of the 24 modes of **TT1**), 5(a), 5(b), 5(c) (bond orders). In the following, we will discuss calculated geometries, energies, vibrational frequencies, and the bond strength of the HB in **TT1** based on the experimental and DFT local mode stretching force constants.

Geometries. In Figure 1(a) and 1(b), ωB97X-D and CCSD(T) geometries of **TT1** and the reference molecules used in this work are given, which compare well with the results of previous investigations [27,30,83], whereas the available experimental data show some deviations due to the fact that they correspond to r_o or r_a structures rather than a r_z structures, which should be closer to the calculated r_e-structures [75,76]. The CCSD(T)/CBS geometries of **TT1** and trans formic acid show typical structural changes caused by double HB. The OH bonds are lengthened from 0.964 to 0.989 Å and the C=O bonds from 1.194 to 1.212 Å whereas the C–O bonds shrink from 1.336 to 1.303 Å. The bond angles have to widen by 1–2° (see Figure 1(a)) to align the two monomers in such a way that the $O - H\cdots O$ angle adjusts to 180°.

Binding energies. The CCSD(T)/CBS HB binding energy $\Delta E(CBS)$ is −18.72 kcal/mol in good agreement with a recent CCSD(T)-F12/CBS value of −18.75 kcal/mol published by Marshall and Sherrill [84]. The corresponding enthalpy $\Delta H(298)$ and free energy differences $\Delta G(298)$ at 298 K are −16.98 and −5.46 kcal/mol where the latter value is due to the large loss in entropy (see Table 1). In this connection, we note that most spectroscopic investigations are done at strongly reduced temperatures and a $\Delta G(10) = -9.83$ kcal/mol may be more relevant [30,33–35]. The calculated cis–trans (C-T) energy difference ΔE of FA is 4.29 kcal/mol and $\Delta H(298) = 4.10$ where the latter value compares well with an approximate observed value of 3.9 kcal/mol [3,4]. It is reasonable to assume that the calculated CCSD(T)/CBS geometries and harmonic vibrational frequencies are reliable although in the case of the second-order properties deviations may be somewhat larger than for the energies.

Table 1 reveals also that the ωB97X-D complex binding energy compares well with the CCSD(T)/aug-cc-pVTZ and even the CCSD(T)/CBS energy where the deviations are less than 10% in case of **TT1**. Hence, it is reasonable to use ωB97X-D results for the discussion of relative energies of **TT1** and the reference molecules used in this work. There is an almost linear relationship between the DFT binding energies and the corresponding HB length for **TT1**, **TT2**, **TT3**, **TC1**, and **TC2**, from which the HB of **CC1** significantly deviates as a result of exchange (steric) repulsion between the CH-hydrogen atoms (see Figure 1(b)). This makes **CC1** inappropriate to be used as a single H-bonded reference for **TT1**.

We also investigated a structure **TT3** obtained from **TT2** by a 180° rotation at the O–H···H bridge, which would be ideally suited as a single H-bonded reference. However, **TT3** turned out to be a transition state of a rotation back to **TT2,** thus we had to exclude **TT3** as a suitable reference molecule. We will show in the following that from all the FAD forms investigated (see Figure 1(a) and 1(b)), the complex **TC2** seems to be best suited as a reference (see discussion below). Finally, we note that, apart from **TT1**, all other FAD complexes investigated in this work should be only observable at low temperatures (see $\Delta G(298)$ values in Table 1).

Normal and local modes. In Table 2, the CCSD(T)/aug-c-pVDZ, aug-c-pVTZ, and CBS harmonic frequencies are compared with the experimental normal mode frequencies [35]. The anharmonicity effects as suggested by the values of $\Delta(Exp - CBS)$ are relatively small apart from the four highest vibrational frequencies, which correspond to the X–H (X = O, C) stretching vibrations (see Table 3 and Figure 3). This was also observed by other authors [34].

In Table 3 and Figure 3, each normal mode is decomposed into local vibrational modes where the local mode contributions are given in % and are coloured according to a colour code also given in Figure 3. The experimental normal and local mode frequencies are listed in Table 4 together with the corresponding coupling frequencies, which are taken from the ACS of Figure 4(a), 4(b), and 4(c). The coupling of the local modes depends on the topology of the molecule in question reflecting the proximity of molecular units and the internal coordinate associate with these units, the similarity of the local mode frequencies, the degree of

Table 2. Harmonic normal mode frequencies ω_μ (cm^{-1}) of the FAD **TT1** calculated using CCSD(T) and the aug-cc-pVXZ basis sets (X = D and T). These frequencies were used to calculate a CBS frequency for each mode using a two-point extrapolation for comparison of harmonic CBS and experimental frequencies. [70]. In the last row, the zero-point energies (ZPE) are given.

μ	Sym.	ω_μ (VDZ)	ω_μ (VTZ)	ω_μ (CBS)	ω_μ (Exp.) [35]	Δ (Exp.–CBS)
24	B_u	3306.7	3308.5	3309.3	3084	−225.3
23	A_g	3209.7	3202.3	3199.2	2949	−250.2
22	B_u	3115.7	3098.1	3090.7	2939	−151.7
21	A_g	3111.8	3095.1	3088.0	2900	−188.0
20	B_u	1750.3	1784.9	1799.5	1746	−53.5
19	A_g	1690.8	1718.5	1730.1	1670	−60.1
18	A_g	1480.6	1497.2	1504.1	1454	−50.1
17	B_u	1454.8	1466.0	1470.8	1415	−55.8
16	A_g	1387.4	1408.7	1417.6	1375	−42.6
15	B_u	1384.0	1405.7	1414.8	1364	−50.8
14	B_u	1231.1	1265.0	1279.3	1218	−61.3
13	A_g	1223.8	1260.0	1275.2	1214	−61.2
12	A_u	1090.6	1131.2	1148.3	1060	−88.3
11	B_g	1067.0	1105.0	1121.0	1050	−71.0
10	A_u	972.8	1017.6	1036.5	922	−114.5
9	B_g	952.0	994.1	1011.8	911	−100.8
8	B_u	698.1	716.2	723.8	698	−25.8
7	A_g	667.6	688.4	697.1	677	−20.1
6	B_u	272.0	279.6	282.8	264	−18.8
5	B_g	251.8	259.4	262.6	242	−20.6
4	A_g	208.6	214.1	216.4	194	−22.4
3	A_u	172.0	189.9	197.4	168	−29.4
2	A_g	168.8	166.5	165.5	161	−4.5
1	A_u	68.3	72.3	74.0	69	−5.0
ZPE [kcal/mol]:		44.2	44.8	45.1	42.5	−2.6

alignment of the local mode vectors, and the mass ratios of the atoms involved in the local modes. This is demonstrated for the four highest experimental frequencies, which according to Table 3 correspond to the OH and CH stretching modes. Normally, one would expect the two OH stretching frequencies to be above the two CH stretching frequencies of **TT1** and for each of these X–H stretching pairs the asymmetric combination above the symmetric combination, the latter of which is observed for the water molecule and the water dimer [56].

For **TT1**, the order of the X–H stretching frequencies is ω_{24}(*asym.OH*), ω_{23}(*sym.CH*), ω_{22}(*asym.CH*), and ω_{21}(*sym.OH*) (see Table 3 and Figure 3; symmetries of the normal modes are given in Table 4). The comparison of the O–H local mode frequencies for **TT1** and trans formic acid (see Supporting Information available online) reveals that the red shift in the OH stretching frequency is 3544–2848 = 696 cm^{-1}, which brings the two local OH stretching frequencies below the local CH stretching frequencies at 2950 cm^{-1} (see Figure 4(a)). Coupling between the O–H (C–H) stretching modes leads to a splitting into the asymmetric above the symmetric combination. The mode vectors are perfectly aligned in both cases, however, the CH modes are only weakly coupled because of spatial separation of the exocyclic CH units. The coupling between the O–H modes is much stronger, which is a result of their incorporation into the framework of the ring. Hence, the B_u-symmetrical OH stretching mode (green in Figure 4(a)) raises to the level of the B_u-symmetrical CH stretching mode and undergoes an avoided crossing (AC1) with the latter at $\lambda = 0.45$.

At AC1, the character of the modes is exchanged so that the upper mode (mode 24) obtains asymmetric OH and the lower mode 22 asymmetric CH stretching character. The frequency of mode 22 is pushed below the symmetric CH stretching mode (mode 23), which almost does not change because of a coupling frequency close to zero (see Table 4 and Figure 4(a)). Noteworthy is the fact that the frequency of mode 21 (symmetric OH) first drops because of mass coupling with the other parts of the molecule, but then increases as a consequence of the topology of the FAD ring. The local mode frequency reflects all electronic effects (delocalisation, hybridisation, anomeric effect, etc.), which means that any ACS diagram and the coupling between the local modes it reveals is a consequence of non-electronic effects (topology of the molecule, mass coupling, avoided crossings, etc.). The latter effects explain the unusual ordering of the XH stretching modes of **TT1** as they are observed experimentally.

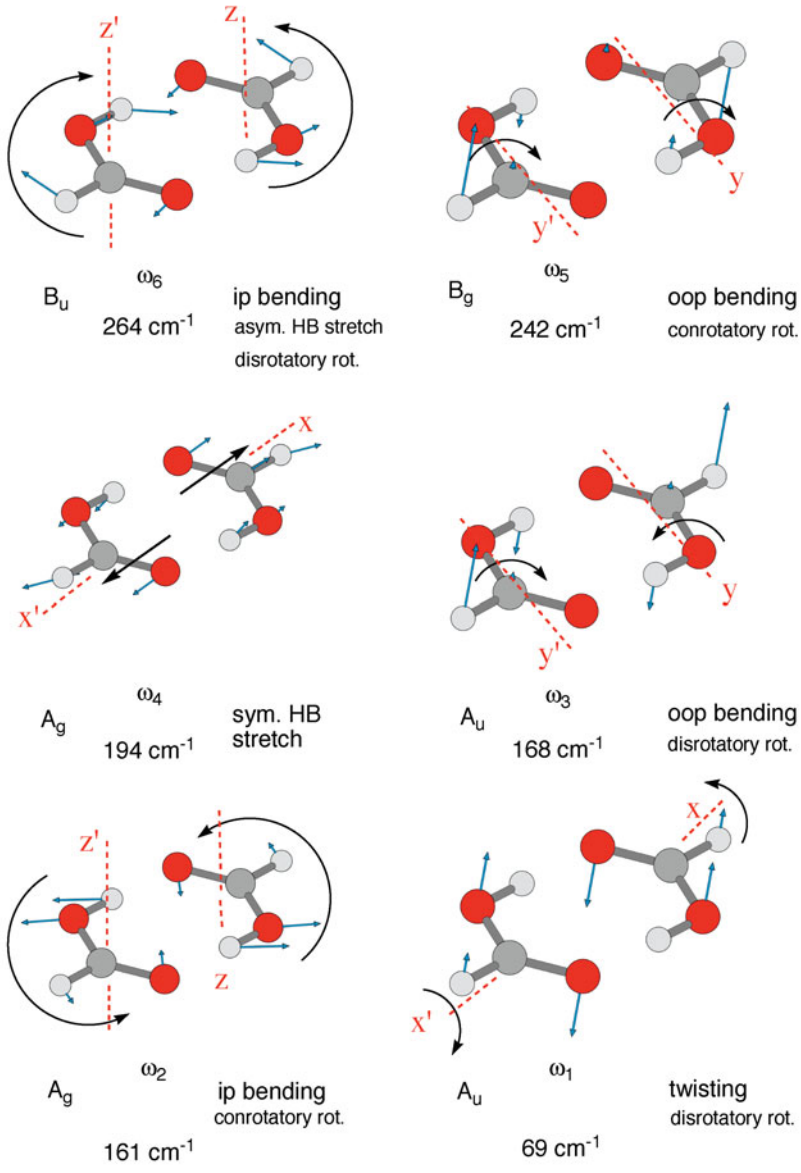

Figure 2. The six intermonomer modes ω_1 to ω_6 of FAD **TT1**. Abbreviations ip, oop, and rot denote in-plane, out-of-plane, and rotation. Frequencies from experiment [35]. Note that there are 12 translations and rotations possible with regard to the principle axes of the monomers of the FAD complex where always pairs of opposite or equally directed translations and conrotatory or disrotatory rotations have to be considered. Of the six possible rotations, the disrotatory one at the *x*-axis leads to the twisting vibration, its conrotatory equivalent to an overall rotation and the two pairs (conrotatory and disrotatory) at *y*- and *z*-axis to modes (3,5) and (2,6). Of the six translations, three lead to an overall movement of the FAD, and the oppositely directed translation along the *x*-axis leads to the HB stretching motion (mode 4) whereas the other two modes mix with two rotations (modes 2 and 5) because of symmetry. It should be noted that the six intermonomer vibrations can be similarly explained by considering the ring as a pseudo-6-membered ring because of the linear O–H···H units. For a C_{2h}-symmetrical 6-ring, there are three out-of-plane motions (mode 5: chair-type; mode 3: boat-type; mode 1: twistboat type) and three in-plane deformation modes [77,79].

The ACS shown in Figure 4(a), 4(b), and 4(c) reveals nine stronger or weaker avoided crossings (AC(mode, mode 2; λ): AC1(22,24; 0.45), AC2(16,18; 0.65), AC3(15,17; 0.5), AC4(14,15; 0.24), AC5(9,11; 0.92), AC6(5,9; 0.14), AC7(6,8; 0.55), AC8(2,4; 0.98), AC9(1,3; 0.92)). These lead to mode mixing and/or a change in the mode character, which can be discussed in detail using the information given in Tables 3 and 4 or Figures 3, 4(a), 4(b), and 4(c). In the following, however, we will focus exclusively on the HB stretching modes, which belong to the six intermonomer

Table 3. Characterisation of the normal modes ω_μ(Exp.) of the FAD **TT1** in terms of the local mode contributions ω_a(Exp.). Except for normal mode 6, only local mode contributions with 5.0% or greater are given.

μ	Characterisation of modes ω_μ(Exp.) in terms of modes ω_a(Exp.)
24	82.6% (O2-H3 / O7-H8), 13.0% (C1-H5 / C6-H10)
23	98.0% (C1-H5 / C6-H10)
22	86.6% (C1-H5 / C6-H10), 11.8% (O2-H3 / O7-H8)
21	93.6% (O2-H3 / O7-H8)
20	72.4% (C1=O4 / C6=O9), 12.4% (C1-O2 / C6-O7), 5.7% O2-C1-H5
19	71.0% (C1=O4 / C6=O9), 10.0% (C1-O2-H3 / C6-O7-H8), 5.0% O2-C1-H5
18	58.2% (C1-O2-H3 / C6-O7-H8), 16.8% (C1=O4 / C6=O9), 12.2% (H8···O4-C1 / H3···O9=C6)
17	67.2% (C1-O2-H3 / C6-O7-H8), 8.7% O2-C1-H5
16	47.9% O9=C6-H10, 35.4% O2-C1-H5
15	42.4% O9=C6-H10, 27.1% O2-C1-H5, 12.0% (C1-O2 / C6-O7), 11.0% (C1-O2-H3 / C6-O7-H8)
14	63.4% (C1-O2 / C6-O7), 15.0% (C1-O2-H3 / C6-O7-H8), 6.9% O2-C1-H5
13	72.8% (C1-O2 / C6-O7), 12.8% (C1-O2-H3 / C6-O7-H8), 5.4% O2-C1-H5
12	69.6% (H3-O2-C1-H5 / H8-O7-C6-H10), 25.2% (O2-H3···O9 / O7-H8···O4)
11	81.2% (H3-O2-C1-H5 / H8-O7-C6-H10), 14.8% (O2-H3···O9 / O7-H8···O4)
10	45.4% (H3-O2-C1=O4 / H8-O7-C6=O9), 44.6% (O2-H3···O9 / O7-H8···O4), 5.0% H3···O9=C6-O7
9	47.8% (O2-H3···O9 / O7-H8···O4), 37.2% (H3-O2-C1=O4 / H8-O7-C6=O9), 14.4% (H3-O2-C1-H5 / H8-O 7-C6-H10)
8	47.1% O9=C6-O7, 28.8% (H3···O9=C6 / H8···O4=C1), 7.8% O2-C1-H5, 5.4% O9=C6-H10
7	64.1% O9=C6-O7, 11.8% O2-C1-H5, 11.6% (C1-O2 / C6-O7), 6.5% O9=C6-H10
6	88.0% (H3···O9 / O4···H8), 4.6% (H3···O9=C6 / H8···O4=C1); 4.6% (H8-O7C6O9 / H3O2C1O4)
5	35.8% (H3-O2-C1=O4 / H8-O7-C6=O9), 30.0% (H3-O2-C1-H5 / H8-O7-C6-H10), 21.6% H3···O9-C 6-O7, 12.6% (O2-H3···O9 / O7-H8···O4)
4	70.2% (H3···O9 / O4···H8), 10.2% (H3···O9=C6 / H8···O4=C1)
3	42.2% (O2-H3···O9 / O7-H8···O4), 26.2% (H3-O2-C1=O4 / H8-O7-C6=O9), 23.0% (H3-O2-C1-H5 / H8-O 7-C6-H10), 8.6% H3···O9=C6-O7
2	31.2% (H3···O9=C6 / H8···O4=C1), 19.0% (C1-O2-H3 / C6-O7-H8), 12.8% (H3···O9 / O4···H8)
1	52.3% H3···O9=C6-O7, 24.4% (H3-O2-C1-H5 / H8-O7-C6-H10), 23.2% (H3-O2-C1=O4 / H8-O7-C6 -O9)

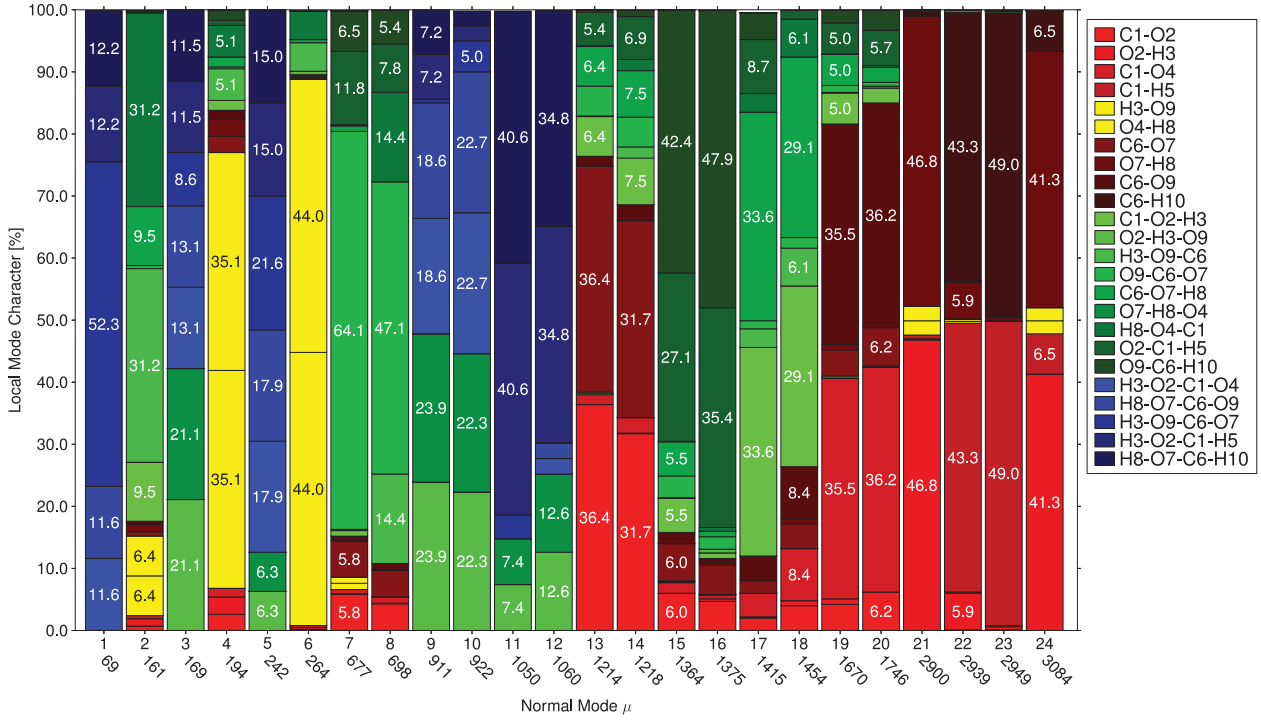

Figure 3. Decomposition of the 24 normal modes of the FAD **TT1** into local modes. Contributions are given in % and are colour-coded for the local modes (identified via the internal coordinate driving it, which is given in the legend on the right).

Table 4. The normal mode symmetries and frequencies ω_μ, the local mode internal parameter, force constants k_a, and frequencies ω_a, the coupling frequencies ω_{coup}, and zero-point energies (ZPE) are given for the FAD **TT1**.

μ	Sym.	ω_μ [cm^{-1}]	#	Param.	k_a [mdyn Å^{-1}][a]	ω_a [cm^{-1}]	ω_{coup} [cm^{-1}]
24	B_u	3084	2	O2-H3	4.530	2848.2	235.8
23	A_g	2949	4	C1-H5	4.766	2949.6	−0.6
22	B_u	2938	10	C6-H10	4.766	2949.6	−11.6
21	A_g	2900	8	O7-H8	4.530	2848.2	51.8
20	B_u	1746	3	C1=O4	10.762	1634.2	111.8
19	A_g	1670	9	C6=O9	10.762	1634.2	35.8
18	A_g	1454	15	C6-O7-H8	0.799	1255.3	198.7
17	B_u	1415	1	C1-O2-H3	0.799	1255.3	159.7
16	A_g	1375	18	O9=C6-H10	0.996	1330.4	44.6
15	B_u	1364	19	O2-C1-H5	1.027	1327.2	36.8
14	B_u	1218	11	C1-O2	6.349	1254.4	−36.4
13	A_g	1214	7	C6-O7	6.349	1254.4	−40.4
12	A_u	1060	24	H8-O7-C6-H10	0.134	711.0	349.0
11	B_g	1050	16	H3-O2-C1-H5	0.134	711.0	339.0
10	A_u	922	17	H8-O7-C6=O9	0.125	599.7	322.3
9	B_g	911	14	O2-H3···O9	0.111	703.4	207.6
8	B_u	698	21	H8···O4=C1	0.334	540.9	157.1
7	A_g	677	23	O9=C6-O7	1.818	865.5	−188.5
6	B_u	264	6	O4···H8	0.256	676.4	−412.4
5	B_g	242	20	H3-O2-C1=O4	0.125	599.7	−357.7
4	A_g	194	5	H3···O9	0.256	676.4	−482.4
3	A_u	168	12	O7-H8···O4	0.111	703.4	−535.4
2	A_g	161	13	H3···O9=C6	0.334	540.9	−379.9
1	A_u	69	22	H3···O9=C6-O7	0.042	289.3	−220.3
ZPE [kcal/mol]:		42.52				43.11	−0.59

[a] Bending force constants are given in (mdyn Å)/rad^2.
[b] ZPE values (second row) are given as the sum of the contribution of the local mode frequencies and the contribution of the coupling frequencies.

modes. These have the lowest vibrational frequencies (see Figure 2).

The intermonomer modes correspond to the A_u-symmetrical twisting mode (ω_1 = 69 cm^{-1}), the A_g-symmetrical in-plane bending mode (ω_2 = 161 cm^{-1}), the A_u-symmetrical out-of-plane bending mode (ω_3 = 168 cm^{-1}), the A_g-symmetrical HB stretching mode (ω_4 = 194 cm^{-1}), the B_g-symmetrical out-of-plane bending mode (ω_5 = 242 cm^{-1}), and the B_u-symmetrical in-plane bending mode (ω_6 = 264 cm^{-1}), where the latter can be viewed as the asymmetrical HB stretch since the rotation indicated in Figure 2 leads to the shortening of one HB and the simultaneous lengthening of the other HB. The differences $\Delta(Exp - CBS)$ suggest that the anharmonicities are all smaller than 30 cm^{-1}. The normal mode decomposition reveals in each case multiple local mode contributions, which is typical of the collective motion of almost all atoms of a monomer relative to those of the atoms of the other monomer. It is possible to define curvilinear coordinates driving this collective motion [79] and by this obtain local modes, which dominate the six intermonomer normal modes, however no attempt was made in this work, which focuses on the strength of the double HB in **TT1**.

Description of the HB stretching vibrations. The two local mode frequencies corresponding to HB stretching are both equal to 676 cm^{-1} whereas the measured HB frequencies appear at 264 (mode 6, asym. HB stretch) and 194 cm^{-1} (mode 4, sym. HB stretch) thus leading to large coupling frequencies of −412 and −482 cm^{-1}, respectively. These normal modes are indeed dominated by HB stretching character (indicated by yellow colour in Figure 3, see also Table 3), however, also contain many small contributions of other local modes. Due to the mode character switch at AC7 and mixing with the H3O9C6 / H8O4C1 bending mode, there is a 10% contribution of bending in mode 4. Direct coupling with the O–H bond stretches leads to small contributions of these modes in 4 and 6 as there are HB stretching contributions in modes 21 and 24. It is obvious from the normal decomposition analysis that there is less mode mixing for the HB stretchings than in the water dimer [56] so that their character dominates modes 4 and 6. The ring structure, however, leads to many small contributions from other modes via weak coupling mechanisms (see Figure 3). Hence, the large negative coupling frequencies (Table 3) are caused for the asymmetric HB stretching by AC7 and mass coupling whereas the symmetric HB

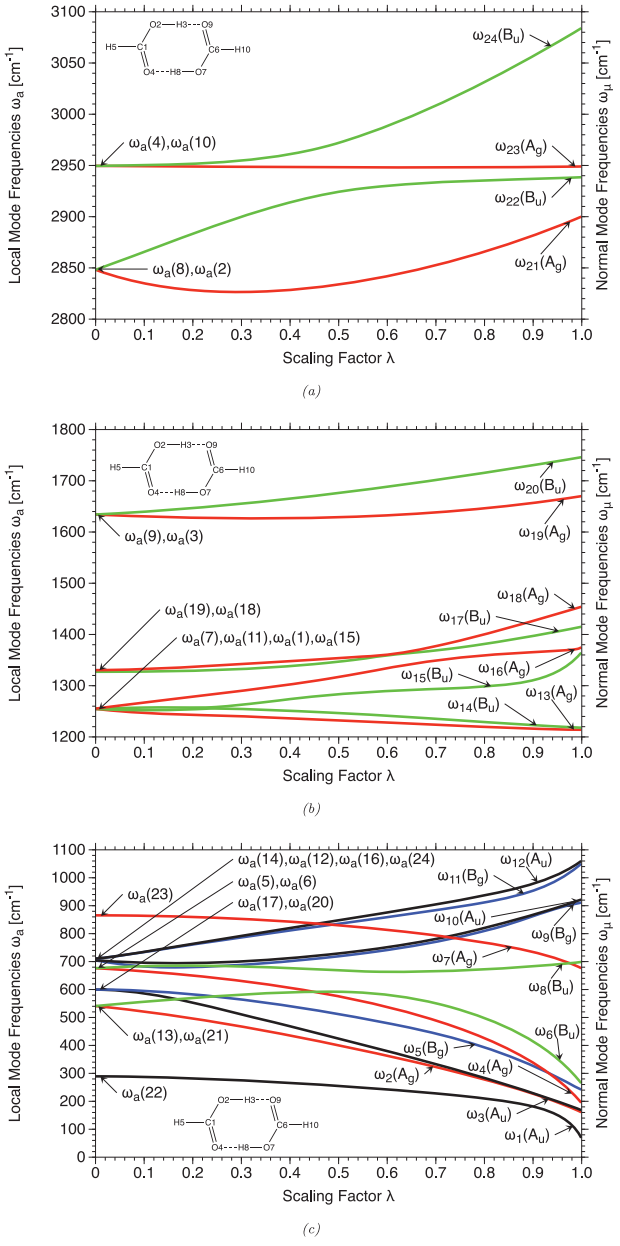

Figure 4. Adiabatic connection scheme relating experimental local mode frequencies (left) utilising experimental normal mode frequencies (right) of the FAD **TT1**. (a) Range from 2800 to 3100 cm^{-1}. (b) Range from 1200 to 1800 cm^{-1}. (c) Range from 0 to 1100 cm^{-1}. The adiabatic connection schemes for calculated harmonic frequencies are similar.

stretching mode 4 is influenced by the coupling between the two local HB modes, mass coupling, and AC8(2,4; 0.98). Since all these factors are significantly different for different H-bonded complexes, there is no basis to determine from measured HB stretching frequencies the strength of the HB or the double HB in **TT1**. This can only be done by utilising the local mode properties.

Strength of the HB. In Table 5, the X–H (X = O, C) and CO bond orders determined for **TT1** and the reference molecules shown in Figure 1(a) and 1(b) are listed. The bond orders have been determined for both calculated and experimentally based stretching force constants k_a. For the purpose of simplifying the analysis of red (blue) shifts in the vibrational frequencies of FAD relative to FA and, by this, also the discussion of the OH and CO bond strength, they are given with regard to the trans formic acid values and also with regard to standard references (water, methanol, and formaldehyde; values in parentheses in Table 5). In addition, the latter bond orders n are shown as a function of k_a in Figure 5(a), 5(b), and 5(c). The comparison of DFT and experimentally based bond orders reveals that they reflect the same relative trends of CO and OH bond strength. Hence, one can conclude that the ωB97X-D bond orders provide a reasonable description of HB.

The HB bond of **TT1** ($n = 0.41$) is clearly much stronger than that of the water dimer ($n = 0.34$; see also Figure 5(a)), which is clearly reflected by the donor O–H bond ($n = 0.88$ vs. 0.98 for the water dimer). This can be easily understood by considering that the transition state of a double proton transfer will be stabilised by the delocalisation of negative charge in the OCO units (beside the well-known π-delocalisation in the O=C−O$^-$ group, there also is an anomeric delocalisation of negative charge from the in-plane lone pair orbital to the $\sigma^\star$(C=O) orbital), which is not possible in the water dimer.

The bond orders of the reference molecules shown in Figure 1(b) make it possible to establish the differences between single HB and double HB. In **CC1**, the single HB is weakened by steric repulsion between 2 H atoms (Figure 1(b)) and therefore, as mentioned above, this FAD structure is not a suitable reference for a single HB. Complexes **TT2** and **TC1** turn out to be stabilised by a second HB between the C=O and H–C group (Figure 1(b)), which has bond order values of 0.28 and 0.31, respectively, revealing that these interactions cannot be neglected. Hence, FAD **TC2** is the only possible reference for the single HB although it includes cis formic acid, which will lead to some change in the nature of the HB. All relevant values for **TC2** are given in the Supporting Information available online. There, a diagram is shown, which presents an almost linear relationship between calculated HB orders n and the HB length. For this relationship, **TC2** takes a middle position among FADs with additional (de)stabilisation effects thus changing the nature of the targeted HB.

By taking **TC2** as a suitable reference molecule for a single HB in an FAD, on can assume its binding energy of −8.1 kcal/mol as a suitable measure of the strength of the HB. However, there will be other small electronic contributions, which influence this value. (i) cis formic acid is less stable than trans formic acid by 4.29 kca/mol (CCSD(T)/CBS, Table 1), which may have a small influence on the HB binding energy of **TC2**. (ii) Deformation of the monomers coupled with rehybridisation effects upon complex formation influence the binding energy. (iii) There

Table 5. Calculated bond orders at the ωB97XD/aug-cc-pVTZ level of theory and experimentally based bond orders. For reasons of simplifying the analysis, the bond orders are given relative to the bond orders of trans formic acid (O–H: $n = 1.00$; C–O: $n = 1.00$; C=O: $n = 2.00$) and relative to the generally accepted references (water: n(OH) = 1.00; methane: n(CH) = 1.00; methanol: n(C–O) = 1.00; formaldehyde: n(C=O) = 2.00) where the latter are given in parentheses.

		r [Å]	k_a [mdyn/Å]	ω_a [cm^{-1}]	n
ωB97XD/aug-cc-pVTZ: XH (X = O, C)					
TT1	O–H	0.996	5.404	3110.4	0.90 (0.88)
	H···O	1.667	0.334	773.3	0.42 (0.41)
TT2	O–H	0.986	6.332	3366.7	0.94 (0.92)
	H···O	1.760	0.265	688.9	0.39 (0.38)
	O4···H10	2.336	0.085	390.2	0.29 (0.28)
	C1–H5	1.097	5.120	3057.3	1.00 (1.01)
	C6–H10	1.093	5.313	3114.3	1.01 (1.02)
TC1	O–H	0.987	6.227	3338.8	0.93 (0.92)
	H3···O9	1.741	0.285	714.9	0.40 (0.39)
	O4···H10	2.275	0.107	437.1	0.31 (0.30)
	C1–H5	1.097	5.126	3058.9	1.00 (1.01)
	C6–H10	1.098	5.082	3045.8	1.00 (1.01)
TC2	O–H	0.974	7.133	3573.6	0.97 (0.96)
	H···O	1.805	0.246	663.3	0.39 (0.37)
CC1	O–H	0.972	7.236	3599.0	0.97 (0.96)
	H···O	1.834	0.205	605.9	0.37 (0.36)
$(H_2O)_2$	O–H	0.966	7.862	3751.7	0.96 (0.98)
	H···O	1.937	0.174	557.5	0.35 (0.34)
trans formic acid	O2–H3	0.966	8.020	3789.2	1.00 (0.99)
	C1–H5	1.096	5.171	3072.5	1.00 (1.01)
cis formic acid	O2–H3	0.960	8.360	3868.6	1.01 (1.00)
	C1–C5	1.102	4.871	2982.1	0.99 (1.00)
H_2O	O–H	0.957	8.554	3913.3	(1.00)
CH_4	C–H	1.088	5.342	3122.8	(1.00)
ωB97XD/aug-cc-pVTZ: CO					
TT1	C–O	1.303	7.263	1340.9	1.15 (1.29)
	C=O	1.214	11.885	1715.3	1.78 (1.80)
TT2	C1–O2	1.318	6.810	1298.4	1.09 (1.24)
	C1=O4	1.204	12.722	1774.6	1.90 (1.89)
	C6–O7	1.323	6.682	1286.1	1.07 (1.22)
	C6=O9	1.207	12.551	1762.6	1.87 (1.87)
TC1	C1–O2	1.316	6.886	1305.6	1.10 (1.25)
	C1=O4	1.205	12.621	1767.6	1.88 (1.88)
	C6–O7	1.330	6.503	1268.8	1.04 (1.20)
	C6=O9	1.201	13.018	1795.2	1.93 (1.92)
TC2	C1–O2	1.322	6.763	1293.9	1.08 (1.23)
	C1=O4	1.203	12.829	1782.1	1.91 (1.90)
	C6–O7	1.332	6.342	1252.9	1.02 (1.18)
	C6=O9	1.193	13.626	1836.6	2.01 (1.98)
CC2	C1–O2	1.329	6.544	1272.8	1.05 (1.20)
	C1=O4	1.195	13.465	1825.7	1.99 (1.96)
	C6–O7	1.328	6.455	1264.1	1.04 (1.19)
	C6=O9	1.193	13.633	1837.1	2.02 (1.98)
trans-FA	C1–O2	1.337	6.189	1237.8	1.00 (1.16)
	C1=O4	1.194	13.517	1829.3	2.00 (1.97)
cis-FA	C1–O2	1.343	6.011	1219.9	0.97 (1.14)
	C1=O4	1.188	14.062	1865.8	2.07 (2.02)
Experimental: XH (X = O, C)					
trans formic acid	O2–H3	0.972	7.014	3543.5	1.00 (1.03)
cis formic acid	O2–H3		7.294	3613.6	0.94 (0.96)
TT1	O–H	1.033	4.530	2847.8	0.81 (0.84)
	H···O	1.670	0.256	676.4	0.35 (0.38)
$(H_2O)_2$	H···O	1.947	0.085	390.4	0.26 (0.28)
	O–H	0.964	7.267	3606.9	0.94 (0.96)
H_2O	O–H	0.957	8.364	3869.6	0.97 (1.00)
CH_4	C–H	1.086	4.895	2989.4	(1.00)

(*Continued*)

Table 5. (*Continued*)

		r [Å]	k_a [mdyn/Å]	ω_a [cm^{-1}]	n
Experimental: CO					
trans formic acid	C1–O2	1.343	5.601	1177.5	1.00 (1.08)
	C1=O4	1.202	13.338	1817.1	2.00 (1.95)
cis formic acid	C1–O2		5.552	1172.4	0.99 (1.08)
	C1=O4		12.835	1782.5	1.94 (1.90)
TT1	C–O	1.320	6.349	1253.7	1.11 (1.18)
	C=O	1.217	10.762	1632.2	1.68 (1.69)
$H_2C=O$	C=O	1.196	13.829	1850.3	(2.00)
H_3COH	C–O	1.413	4.972	1109.4	(1.00)

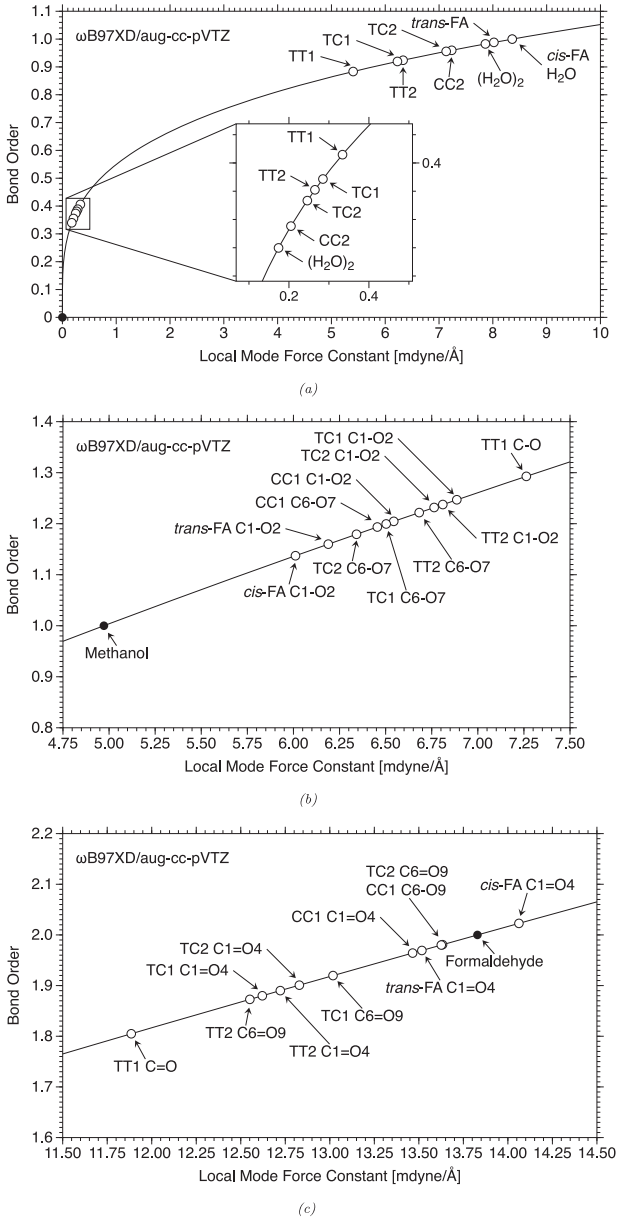

Figure 5. OH (a) and CO bond orders (b and c) based on ωB97X-D/aug-cc-pVTZ calculations.

are also, independent of the HB, electrostatic interactions between the monomers in **TT1**, which influence the binding energy.

The HB in **TC2** (8.1 kcal/mol, Table 1) is 3 kcal/mol stronger than the HB in the water dimer (5.0 kcal/mol [56]). This corresponds to an increase in the bond order from 0.34 to 0.37. Another increase by 0.04 in the bond order to $n = 0.41$ for the double HB in **TT1** should imply an increase in the energy by ca 10% or 0.8 kcal/mol. Hence, one can expect a total HB-binding energy of 17.7 kcal/mol, which is in the range of calculated values (Table 1) and acceptable considering the influence of other electronic effects on the complex binding energy. This means that the delocalisation effect in the O=C–O unit, discussed above, leads to a stabilisation of each HB by 3 kcal/mol, whereas the formation of two each other indirectly supporting HBs in a ring structure adds in total about 1.6 kcal/mol or 10% to the total stabilisation energy.

The double HB in **TT1** affects also the strength of the CO bonds as reflected by the corresponding bond orders (Table 5 and Figure 5(b) and 5(c)). These increase for the C–O bonds by 15% relative to the value of trans formic acid, however, decrease by 22% in the case of the C=O bonds (Table 5). The corresponding values for **TC2** are just 8 and 9%, again indicating the difference between a single HB and a double HB. Red and blue shift in the experimental CO local mode stretching frequencies are given by the following values: ω_a(C=O, **TT1**) = 1634 vs ω_a(C=O, trans formic acid) = 1817 (red shift) and ω_a(C−O, **TT1**) = 1254 vs ω_a(C−O, trans formic acid) = 1177 cm^{-1} (blue shift). Shifts of -183 (C=O) and 77 cm^{-1} (C–O) are substantial and reveal that, apart from the red shift of the O–H stretching frequency also the CO bonds provide a sensitive measure of the type of HB (see data in Supporting Information available online).

4. Conclusions

This work provides a detailed analysis of the experimental vibrational spectrum of the FAD **TT1** by determining 24 local vibrational modes and the corresponding local mode

force constants. This facilitates an analysis of HB in FADs with the help of vibrational spectroscopy and leads to the following results:

(1) Both local HB stretching frequencies of **TT1** are at 676 cm^{-1} and thereby 412 and 482 cm^{-1} higher than the measured frequencies identified to represent HB stretching modes. The lowering of the local HB frequencies is a result of (i) mass coupling, (ii) the topology of the FAD ring in **TT1**, and (iii) avoided crossing between modes of the same symmetry. Contrary to the observations made in the case of the water dimer [56], a change in the anharmonic effects plays only a minor role.

(2) The six intermonomer modes have been analysed and set into relationship to local modes driven by suitable internal coordinates. In each of these cases, the normal mode is a mixture of several local modes. The local modes assigned to the intermonomer modes have coupling frequencies between -220 and -535 cm^{-1} as a result of mass coupling and avoided crossings.

(3) The strength of the double HB of **TT1** is a result of two specific electronic effects. (i) Charge delocalisation in the O=C–O units strengthens HB by about 3 kcal/mol relative to the HB strength in the water dimer as is suggested by the complexation energy of 8.1 kcal/mol of the reference molecule **TC2** possessing a single HB. (ii) The synergy of the concerted formation of double HB leads to another stabilisation of ca. 1.6 kcal/mol.

(4) HB also affects the strength of the CO bonds. It causes a weakening of the C=O and a strengthening of the C–O bonds as is reflected by the corresponding differences in the calculated geometries and local mode frequencies (C=O red shift: -183 cm^{-1}; C–O blue shift: 77 cm^{-1}) of **TT1** and trans formic acid. Hence, the measured CO stretching frequencies provide, via red or blue shifts, a sensitive measure for the electronic consequences of the HB, which has so far not been exploited. However, one has to note that this measure will be only reliable if normal modes are converted to local modes.

(5) We have demonstrated how the unusual order of the 4 X–H (X = O, C) stretching frequencies and their individual values are results of (i) the 696 cm^{-1} red shift in the O–H stretching frequencies, (ii) the large coupling of the O–H stretching modes compared to the very small coupling of the C–H stretching modes, (iii) the resulting avoided crossing between the B_u-symmetrical OH and CH stretching modes, and (iv) the topology of the **TT1** ring.

This work demonstrates that modern vibrational spectroscopy is a valuable tool to analyse structure and bonding in H-bonded complexes. This tool becomes even more powerful with the help of the local vibrational modes and appropriate quantum chemical calculations. The investigation of FAD clearly supports the usefulness of local mode force constants as reliable bond strength descriptors. We note that in the way experimental techniques improve vibrational frequencies can be measured that refer to the zero vibrational levels and are no longer dominated by hot bands. This will make a direct comparison with anharmonically corrected calculated frequencies possible.

Supporting Information

Additional information in form of 20 tables and 5 figures containing the results for the reference molecules are given in the Supporting Information. This material is available free of charge via the Internet at http://www.informaworld.com.

Acknowledgements

This work was financially supported by the National Science Foundation, Grant CHE 1152357. We thank SMU for providing computational resources.

References

[1] G. Gilli and P. Gilli, *The Nature of the Hydrogen Bond- IUCr Monographs on Crystallography - 23* (Oxford University Press, New York, 2009).
[2] S.J. Grabowski, *Hydrogen Bonding - New Insights, in Challenges and Advances in Computational Chemistry and Physics* (Springer, New York, 2006).
[3] W.H. Hocking, Z. Naturforsch. A. **31**, 1113 (1976).
[4] J. Chao and B.J. Zwolinski, Equilibrium **364**, 367 (1978).
[5] L. Khriachtchev, J. Mol. Struct. **880**, 14 (2008).
[6] M. Petterson, E. Macoas, L. Khriachtchev, J. Lundell, R. Fausto, and M. Räsänen, J. Chem. Phys. **117**, 9095 (2002).
[7] A. Domanskaya, K. Marushkevich, L. Khriachtchev, and M. Räsänen, J. Chem. Phys. **130**, 154509 (2009).
[8] J.F. Jia, H.S. Wu, and Y. Mo, J. Chem. Phys. **136**, 144315 (2012).
[9] A.G. Császár, W.D. Allen, and H.F. Schaefer, J. Chem. Phys. **108**, 9751 (1998).
[10] Y.T. Chang, Y. Yamaguchi, W.H. Miller, and H.F. Schaefer, III, J. Am. Chem. Soc. **109**, 7245 (2001).
[11] I. Yokoyama, Y. Miwa, and K. Machida, J. Phys. Chem. **95**, 9740 (1991).
[12] G.M. Florio, T.S. Zwier, E.M. Myshakin, K.D. Jordan, and E.L. Sibert, J. Chem. Phys. **118**, 1735 (2003).
[13] C.S. Tautermann, A.F. Voegele, and K.R. Liedl, J. Chem. Phys. **120**, 631 (2004).
[14] G.V. Mil'nikov, O. Kühn, and H. Nakamura, J. Chem. Phys. **123**, 074308 (2005).
[15] D. Luckhaus, J. Phys. Chem. A **110**, 3151 (2006).
[16] I. Matanović, N. Došlić, and O. Kühn, J. Chem. Phys. **127**, 014309 (2007).
[17] G.L. Barnes, S.M. Squires, and E.L. Sibert, J. Phys. Chem. B **112**, 595 (2008).

[18] G.L. Barnes and E.L. Sibert, III, J. Mol. Spec. **249**, 78 (2008).
[19] G.L. Barnes and E.L. Sibert, J. Chem. Phys. **129**, 164317 (2008).
[20] A.M. da Silva, S. Chakraborty, and P. Chaudhuri, Int. J. Quantum Chem. **112**, 2822 (2011).
[21] D. Yang, Y. Yang, and Y. Liu, Cent. Euro. J. Chem. **11**, 171 (2012).
[22] J. Novak, M. Mališ, A. Prlj, I. Ljubić, O. Kühn, and N. Došlić, J. Phys. Chem. A **116**, 11467 (2012).
[23] M. Gantenberg, M. Halupka, and W. Sander, Chem. Eur. J. **6**, 1865 (2000).
[24] F. Madeja, M. Havenith, K. Nauta, R. Miller, J. Chocholousova, and P. Hobza, J. Chem. Phys. **120**, 70554 (2004).
[25] A. Olbert-Majkut, J. Ahokas, J. Lundell, and M. Pettersson, Chem. Phys. Lett. **468**, 76 (2009).
[26] F. Ito, J. Chem. Phys. **128**, 114310 (2008).
[27] R.M. Balabin, J. Phys. Chem. A **113**, 4910 (2009).
[28] E.M.S. Macoas, P. Myllyperkiö, H. Kunttu, and M. Pettersson, J. Phys. Chem. A **113**, 7227 (2009).
[29] K. Marushkevich, L. Khriachtchev, J. Lundell, and M. Räsänen, J. Am. Chem. Soc. **128**, 2060 (2006).
[30] K. Marushkevich, L. Khriachtchev, J. Lundell, A. Domanskaya, and M. Räsänen, J. Phys. Chem. A **114**, 3495 (2010).
[31] K. Marushkevich, M. Siltanen, M. Räsänen, L. Halonen, and L. Khriachtchev, J. Phys. Chem. Lett. **2**, 695 (2011).
[32] K. Marushkevich, L. Khriachtchev, M. Räsänen, M. Melavuori, and J. Lundell, J. Phys. Chem. A **116**, 2101 (2012).
[33] P. Zielke and M.A. Suhm, Phys. Chem. Chem. Phys. **9**, 4528 (2007).
[34] Z. Xue and M.A. Suhm, J. Chem. Phys. **131**, 054301 (2009).
[35] F. Kollipost, R.W. Larsen, A.V. Domanskaya, M. Nörenberg, and M.A. Suhm, J. Chem. Phys. **136**, 151101 (2012).
[36] M. Kanakidou, J.H. Seinfeld, S.N. Pandis, I. Barnes, F.J. Dentener, M.C. Facchini, R. Van Dingenen, B. Ervens, A. Nenes, and C.J. Nielsen, Atmos. Chem. Phys. **5**, 1053 (2005).
[37] J. Zhao, A. Khalizov, R. Zhang, and R. McGraw, J. Phys. Chem. A **113**, 680 (2009).
[38] E. Braude and F. Nachod, *Determination of Organic Structures by Physical Methods* (Academic Press, New York, 1955).
[39] W. Keene and J. Galloway, Tellus B **40**, 322 (1988).
[40] G. Jeffrey, *An Introduction to Hydrogen Bonding* (Oxford University Press, New York, 1997).
[41] G. Jeffrey and W. Saenger, *Hydrogen Bonding in Biological Structures* (Springer-Verlag, Berlin, 1991).
[42] S. Scheiner, *Hydrogen Bonding: A Theoretical Perspective* (Oxford University Press, New York, 1997).
[43] P.E. Pihko, *Hydrogen Bonding in Organic Synthesis* (Wiley, New York, 2009).
[44] K. Müller-Dethlefs and P. Hobza, Chem. Rev. **100**, 143 (2000).
[45] T. Steiner, Angew. Chem. Int. Ed. **41**, 48 (2002).
[46] N. Belkova, E. Shubina, and L.M. Epstein, Acc. Chem. Res. **38**, 624631 (2005).
[47] M. Meot-Ner, Chem. Rev. **105**, 213 (2005).
[48] P. Munshi and T. Row, Cryst. Rev. **11**, 199 (2005).
[49] P. Gilli, L. Pretto, V. Bertolasi, and G. Gilli, Acc. Chem. Res. **42**, 33 (2009).
[50] S. Grabowski, Chem. Rev. **111**, 2597 (2011).
[51] Z. Konkoli and D. Cremer, Int. J. Quant. Chem. **67**, 1 (1998).
[52] Z. Konkoli and D. Cremer, Int. J. Quant. Chem. **67**, 29 (1998).
[53] W. Zou, R. Kalescky, E. Kraka, and D. Cremer, J. Chem. Phys. **137**, 084114 (2012).
[54] W. Zou, R. Kalescky, E. Kraka, and D. Cremer, J. Mol. Model. 2012 (unpublished).
[55] M. Freindorf, E. Kraka, and D. Cremer, Int. J. Quantum Chem. **112**, 3174 (2012).
[56] R. Kalescky, W. Zou, E. Kraka, and D. Cremer, Chem. Phys. Lett. **554**, 243 (2012).
[57] J. Decius, J. Chem. Phys. **38**, 241 (1963).
[58] S.J. Cyvin, *Molecular Vibrations and Mean Square Amplitudes*. (Universitetsforlaget, Oslo, 1971), p. 68–73.
[59] M. Vijay Madhav and S. Manogaran, J. Chem. Phys. **131**, 174112 (2009).
[60] D. Cremer, J.A. Larsson, and E. Kraka, in *Theoretical and Computational Chemistry, Volume 5, Theoretical Organic Chemistry*, edited by C. Parkanyi (Elsevier, Amsterdam, 1998), p. 259.
[61] Z. Konkoli, D. Cremer, and E. Kraka, J. Comput. Chem. **18**, 1282 (1997).
[62] J.D. Chai and M. Head-Gordon, Phys. Chem. Chem. Phys. **10**, 6615 (2008).
[63] J.D. Chai and M. Head-Gordon, J. Chem. Phys. **128**, 084106 (2008).
[64] T.J. Dunning, J. Chem. Phys. **90**, 1007 (1989).
[65] D. Woon and T.J. Dunning, J. Chem. Phys. **98**, 1358 (1993).
[66] S. Boys and F. Bernardi, Mol. Phys. **19**, 553 (1970).
[67] S. Simon, M. Duran, and J. Dannenberg, J. Chem. Phys. **105**, 11024 (1996).
[68] K. Thanthiriwatte, E. Hohenstein, L. Burns, and C. Sherrill, J. Chem. Theor. Comp. **7**, 88 (2011).
[69] K. Raghavachari, G.W. Trucks, J.A. Pople, and M. Head-Gordon, Chem. Phys. Lett. **157**, 479 (1989).
[70] A. Halkier, T. Helgaker, P. Jorgensen, W. Klopper, H. Koch, J. Olsen, and A.K. Wilson, Chem. Phys. Lett. **286**, 243 (1998).
[71] J.D. McMahon and J.R. Lane, J. Chem. Phys. **135**, 154309 (2011).
[72] R.M. Balabin, J. Chem. Phys. **132**, 211103 (2010).
[73] X.W. Sheng, L. Mentel, O.V. Gritsenko, and E.J. Baerends, J. Comput. Chem. **32**, 2896 (2011).
[74] E. Macoas, J. Lundell, M. Petterson, L. Khriachtchev, R. Fausto, and M. Räsänen, Mol. Spectrosc. **219**, 70 (2003).
[75] G.H. Kwei and R.F. Curl, J. Chem. Phys. **32**, 1592 (1960).
[76] A. Almenningen, O. Bastiansen, and T. Motzfeldt, Acta Chem. Scand. **23**, 2848 (1969).
[77] D. Cremer and J.A. Pople, J. Am. Chem. Soc. **97**, 1354 (1975).
[78] D. Cremer and K.J. Szabo, in *Stereochemical Analysis, Conformational Behavior of Six-Membered Rings, Analysis, Dynamics, and Stereoelectronic Effects*, edited by E. Juaristi (New York, VCH Publishers, 1995), p. 59.
[79] W. Zou, D. Izotov, and D. Cremer, J. Phys. Chem. **115**, 8731 (2011).
[80] K.P. Huber and G. Herzberg (Van Nostrand Reinholdl, New York, 1979).
[81] K. Kawaguchi and E. Hirota, J. Chem. Phys. **87**, 6838 (1987).
[82] T. Shimanouchi, *Tables of Molecular Vibrational Frequencies Consolidated Volume I* (National Bureau of Standards, Washington, DC, 1972).
[83] M.S. Marshall, L.A. Burns, and C.D. Sherrill, J. Chem. Phys. **135**, 194102 (2011).
[84] M.S. Marshall and C.D. Sherrill, J. Chem. Theory Comput. **7**, 3978 (2011).